The influence of coastal upwelling and a river plume on the subsurface chlorophyll maximum over the shelf of the northeastern South China Sea

Zhongming Lu [a], Jianping Gan [a,*], Minhan Dai [b], Anson Y.Y. Cheung [a]

[a] Division of Environment and Department of Mathematics, Hong Kong University of Science and Technology, Kowloon, Hong Kong, China
[b] State Key Laboratory of Marine Environmental Science, Xiamen University, Xiamen, China

A R T I C L E   I N F O

A B S T R A C T

Frequently observed subsurface chlorophyll maximum (SCM) contributes substantial biomass to the waters over the continental shelf of the northeastern South China Sea (NSCS) but it has not been sufficiently investigated. In this study, observations and a three-dimensional coupled physical–biological numerical model were utilized to investigate the characteristics of the SCM under strong controls of coastal upwelling circulation and the Pearl River plume in the NSCS. The model captures the observed characteristics of the SCM in the NSCS reasonably well. Both the depth and intensity of the SCM are spatially variable and regulated by the variable upwelling circulation and associated plume distribution over the complex shelf topography. In nearshore waters, the SCM shoals and weakens towards the coast as a result of the upwelling of high nutrient low chlorophyll deep water while surface productivity is enhanced. The intensity of the SCM weakens when the surface layer is covered by the river plume because of the substantial reduction of photosynthetic active radiation (PAR). Strengthening upwelling-favorable wind weakens the intensity of the SCM due to dilution by the enhanced mixing, but the SCM depth remains relatively stable in the offshore water as a result of no apparent shift of the nutricline. Changing incident PAR leads to an interactive response in chlorophyll concentration, nutricline, and the depth of the SCM.

© 2010 Elsevier B.V. All rights reserved.

1. Introduction

Subsurface chlorophyll maximum (SCM; also known as the deep chlorophyll maximum) have been received substantial attention since the earliest reports (Riley et al., 1949; Steele and Yentsch, 1960; Anderson, 1969) because of the significant contribution of this SCM layer to the water column biomass and primary production, especially in oligotrophic regions of tropical and subtropical ocean (Furuya, 1990; Takahashi and Hori, 1984; Fennel and Boss, 2003). Takahashi and Hori (1984) suggested that ~55% of the total chlorophyll in a water column of the western North Pacific Ocean accumulated in the SCM layer. Estrada (1985) estimated that the SCM contributed to up to 30% of the total summer primary production in the Catalano-Balearic Sea.

SCMs are believed to be typically developed near nutricline in stratified water column and its formation, development, and sustenance are controlled by a suite of physical processes spanning from wind and tidal mixing (Chen et al., 1988), internal waves (Holloway and Denman, 1989), dynamics of the seasonal thermocline (Murty et al., 2000), to the mesoscale instabilities of the shelf/slope front (Flos and Tintore, 1990). These processes are associated with nutrient supplies into the upper ocean.

SCMs are also believed to be formed in the nutricline by the accumulation of phytoplankton that sinks from the surface because those phytoplanktonic cells sink faster in nutrient depleted surface layers (Bienfang, 1980; Parslow et al., 2001). The adaptation of chlorophyll to the phytoplankton biomass ratio in response to variations of PAR and nutrient availability in the water column is another possible reason of the SCM's formation (Steele, 1964; Cullen, 1982; Parslow et al., 2001; Fennel and Boss, 2003). A vertically variable grazing rate can also play an important role during the formation of the SCM. Higher grazing pressure in the upper layer than at the thermocline may lead to the formation of the SCM near the thermocline (Kononen et al., 1998).

While the formation and sustenance of the SCMs are therefore clearly dependent on physical and biological settings of an individual system (Fennel and Boss, 2003; Huisman et al., 2006), SCMs may be subject to substantial variability in time and space, which deserves further investigations. This is particularly true in coastal systems, where physical and biological processes interplay in a very complex way, but research that addresses the process and variability of the SCM under the control of coastal circulation and associated biological response is relatively scarce.

Over the continental shelf in the northeastern South China Sea (NSCS), southwesterly monsoon winds produce coastal upwelling

* Corresponding author. Tel.: +852 23587421; fax: +852 23581582.
E-mail address: magan@ust.hk (J. Gan).

during the summer. The upwelling circulation exhibits strong variability both in alongshore and cross-shore directions because of highly variable shelf topography and the buoyant Pearl River plume (Gan et al., 2009a,b). Biological conditions are largely regulated by the upwelling and plume coastal dynamics (Gan et al., 2010). With a well-mixed inner shelf, the intensive exchange between the mid and inner shelves, and the existence of the river plume, the NSCS represent a unique system under the co-influence of coastal upwelling and estuarine plume. This study investigates the processes and associated mechanisms that govern the variability of the SCM in a dynamic environment highly controlled by upwelling and a river plume in the NSCS. Combined with observations, a coupled physical–biological model that resolves wind-driven coastal upwelling, the river plume, and the biological processes of the SCM is adopted towards such a goal of the present study.

2. Methods

2.1. Study area

The NSCS has a broad continental shelf with a variable offshore extension that ranges from 150 km to 300 km (Fig. 1). The hydrodynamic conditions in the NSCS are shaped by the complex geometry of the coastline and bottom topography as well as by the southwest and northeast monsoons during summer and winter, respectively. The strong freshwater discharge from the Pearl River adds additional complexity to the hydrological environment. The SCM has been frequently reported in the region, either in near-shore waters (Ning et al., 2004) or over the continental shelf, generally, between 30 m and 75 m (Cai et al., 2002; Peng et al., 2006). In the latter region, the phytoplankton biomass and nutrient concentration in the surface water are very low and vertical stratification exists most of time.

During the summer, coastal upwelling frequently occurs. It is driven by the strong southwest monsoon and intensified by shelf topography (Gan et al., 2009a). At the same time, the Pearl River discharge with rate over 16,000 $m^{-3} s^{-1}$ influences the broad region over the shelf (Gan et al., 2009b). There is significant interaction between upwelling circulation and the river plume over the shelf of the NSCS, in which wind-driven upwelling circulation shapes the river plume over the continental shelf and the buoyancy in the plume modulates the flow field. The biological response in this region is mainly regulated by the combined effects of the coastal upwelling and river discharge (Gan et al., 2010), which make the SCM highly variable over the continental shelf.

2.2. Observations

Field observations were conducted during the summer monsoon season. The locations of the field sites are shown in Fig. 1. Stations A1 to A10 along section A were sampled from July 20 to 24, 2004. Station B3 on section B was sampled on July 9, 2004. Both cruises, aboard the R/V Yanpin II, are part of Project CAR-TTT (CARbon Transfer, Transport, and Transformation). Other stations were sampled from June 30 to July 8, 2008, aboard the R/V Shiyan III as part of SCOPE (South China Sea Coastal Oceanographic Process Experiment) (Gan et al., 2010). Salinity, temperature, pressure, PAR, and chlorophyll-a (Chl *a*) data were collected with an SBE-19-plus Conductivity–Temperature–Depth/Pressure (CTD) unit with additional PAR and chlorophyll fluorescence sensor (Sea-Bird Co.). The CTD and additional sensors were calibrated before each cruise. All the above parameters had a sampling rate of 1 scan every 0.5 s, and then averaged to 1 set of data every 1 m. Nitrate (NO_3^-) was determined by a flow injection analyzer (Tri-223 autoanalyzer) provided by S.C. Pai of Taiwan University (Cai et al., 2004).

2.3. Coupled physical–biological model

We used a coupled physical–biological model to simulate the physics and the ecosystem over the continental shelf of the NSCS. The model domain extends from 15.99°N, 108.17°E in the southwest to 25.81°N, 119.54°E in the northeast. The physical model is the Regional
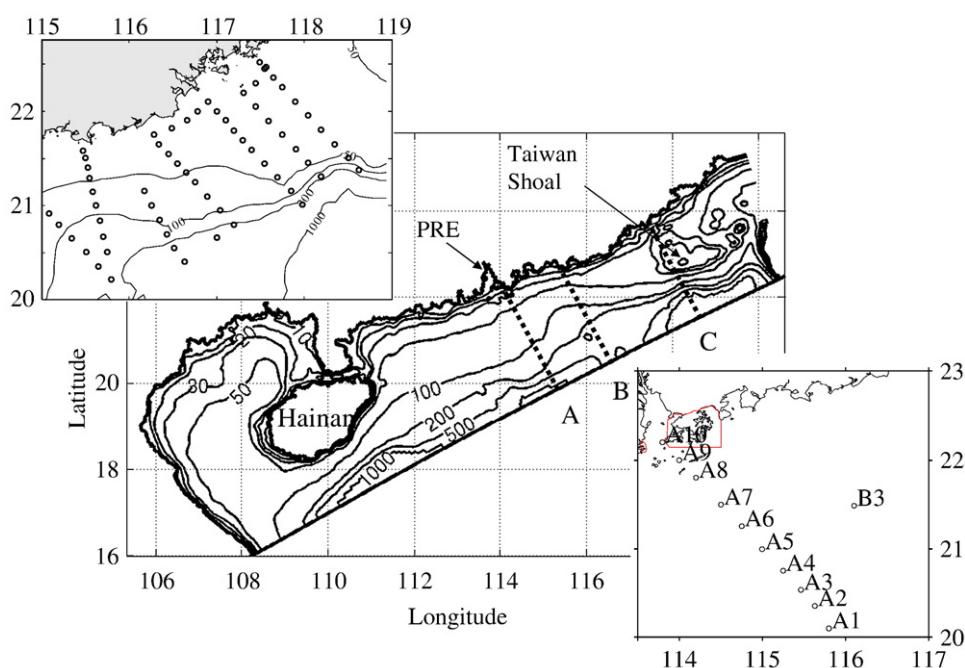
Fig. 1. Map and the model domain of the NSCS with isobaths of 20, 50, 100, 200, 500, and 1000 m. The dashed lines marked with A, B, and C denotes three representative cross-sections with distinct topographical and hydrological conditions. The open circles in the upper left panel represent the observation sites of project SCOPE; in the lower right panel they represent the observation sites of project CAR-TTT.
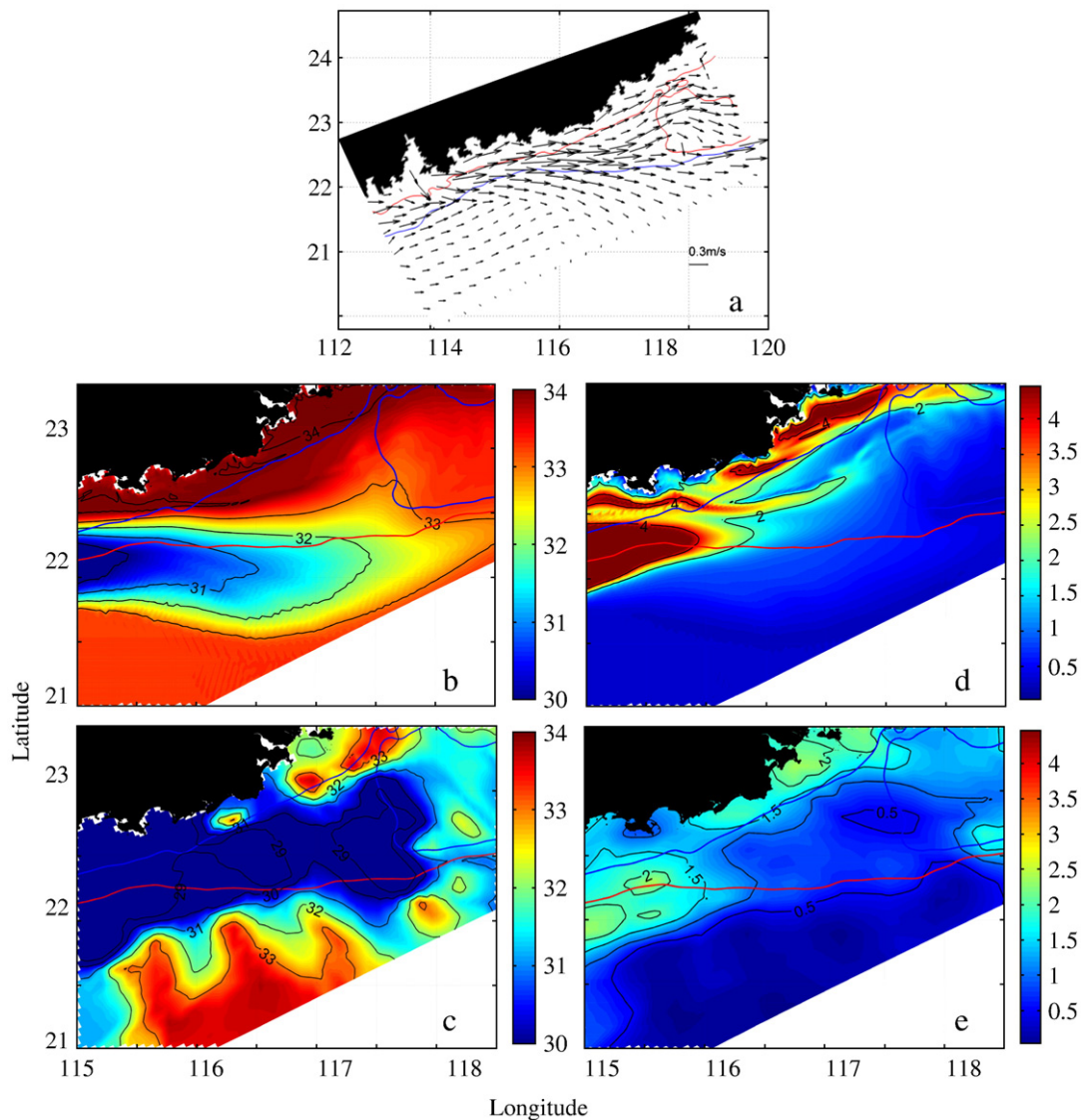
Fig. 2. Ensembles of (a) simulated surface velocity; (b) and (c) simulated and observed surface salinity (PSU); (d) and (e) simulated and observed surface chlorophyll (µg L^{-1}). All field measurements are sampled from June 30 to July 8, 2008.

Ocean Modeling System (ROMS) (Shchepetkin and McWilliams, 2005; Haidvogel et al., 2008) for three-dimensional, time-dependent oceanographic flows governed by hydrostatic primitive equations. A local closure scheme based on the level-2.5 turbulent kinetic energy equations by Mellor and Yamada (1982) was adopted in the vertical mixing parameterization. The model has an average horizontal resolution of 3 km and 30 vertical levels. The water depths, $h(x,y)$, are obtained by merging ETOPO2 (1/30°) data from the National Geophysical Data Center (USA) with water depths digitized from navigation charts published by China's Maritime Safety Administration. As a process-oriented study, the dynamic characteristics of summer upwelling conditions in the NSCS were simulated by forcing the model with spatially uniform, southwesterly wind stress of 0.025 Pa and initialized with horizontally uniform salinity and temperature profiles obtained from field measurements at station A1 (Fig. 1). The discharge rate of the Pearl River was set to the typical summer value of 16,500 m^3 s^{-1}. More detailed model settings and conditions are reported in Gan et al. (2009a,b).

The biological model is coupled to the physical model with identical temporal and spatial resolution. It is a Fasham-type ecosystem model (Fasham et al., 1990) and is included in the ROMS

as a sub-model (Fennel et al., 2006). This biological model includes 6 compartments: nitrate (N), ammonium (A), phytoplankton (P), zooplankton (Z), large detritus (LD), and small detritus (SD). A variable chlorophyll (Chl a) to phytoplankton ratio that depends on PAR and NO$_3$ was applied. The ecosystem model equations are presented in Appendix A. The parameters used in this model are presented in Appendix B. Most of them were taken from the ROMS (Fennel et al., 2006). Several parameters were adapted to the study area (Gan et al., 2010).

The biological model was also initialized with horizontally uniform profiles for all variables. An idealized solar radiation (I) with a diurnal cycle was used. The radiation in daytime (covering 16 h) was calculated by the following equation according to observation:

$$I = 450* \sin (t*\pi / 16) \tag{1}$$

Solar radiation at night was set to 0. The initial profiles of NO$_3$ and chlorophyll were obtained from observations at A1 (Fig. 1). The initial profiles of other biological parameters were taken from a 1-D model after a 1-year run with small background diffusivity and without sinking (Spitz et al., 2005; Gan et al., 2010). The initial NO$_3$ in the river

discharge was set to 60 µmol L^{-1} following Cai et al. (2004). The detailed description of the model equations, parameters, initializations, and settings can be found in Gan et al. (2010) and Fennel et al. (2006).

3. Results

3.1. Surface characteristics of river plume and upwelling

Coastal upwelling and the formation of the upwelling jet are produced by the southwesterly monsoon wind over the shelf in the NSCS during the summer (Fig. 2a). The upwelling current mainly flows along the isobath of shelf topography due to geostrophy. The salinity field is characterized by the eastward-flowing river plume over the mid-shelf region along the 50 m isobath and by high salinity upwelled waters next to the coast over the inner shelf (Fig. 2b, c). The simulated physical field represents typical upwelling characteristics as shown by (Gan et al., 2009a,b) and by field measurements.

Stimulated by the high nutrients concentration (represented by NO$_3$ in this model), a phytoplankton bloom occurs, characterized by two distinct high Chl *a* centers in the plume and in the intensified
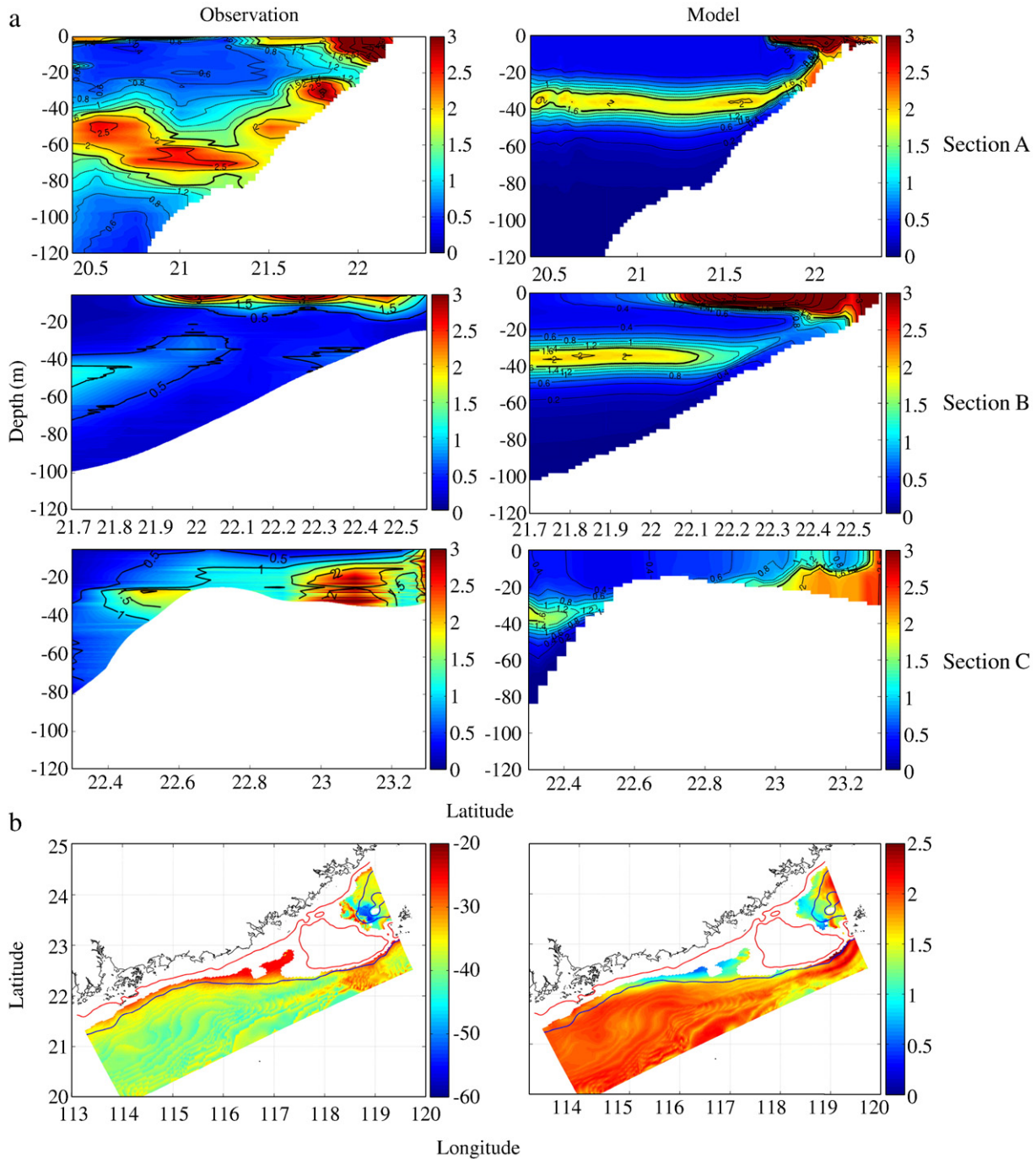
Fig. 3. (a) Qualitatively comparisons of observed (left column) and simulated (right column) SCM along sections A, B, and C, respectively. The measurements of section A were conducted from July 20 to 24, 2004, and sections B and C were sampled from July 1 to 8, 2008; (b) Horizontal distributions of the depth (m) (left) and intensity (right) of the simulated SCM (µg L^{-1}), respectively. All simulated results are for day 30.

upwelling region (Fig. 2d). Field observations reveal identical features (Fig. 2e), which therefore suggests that our model well captured the biological response to the nutrient supplies. Note that the phytoplankton bloom generally extends farther offshore than the NO_3, but less than the salinity in the plume and in the upwelled waters, due to the combined effect of water motion and time lag response among nutrients, phytoplankton, and zooplankton (Gan et al., 2010).

3.2. Structures of SCM

The interaction between the upwelling circulation and the complex bottom topography and coastline results in high variability of wind-driven coastal upwelling over the inner and mid-shelf regions (Gan et al., 2009a). Moreover, considering the interaction of the upwelling with the Pearl River plume, the horizontal and vertical hydrodynamic conditions of this region are extremely complex. To show the response of the SCM to the upwelling-plume field in the NSCS, Chl a vertical structures and their alongshore variation are shown by three representative cross-shelf sections along the shelf of the NSCS (Fig. 3a). Significant SCMs exist in both simulated and observed fields in all three sections at depths between 40 and 50 m. Forced with the prevailing upwelling wind, the characteristics of the simulated SCMs are qualitatively similar to the observed ones. This suggests that the alongshore variation of the SCM shown in the sections is a robust characteristic of the NSCS.

Located in the PRE, the river plume in section A generates a nearly stationary bulge of freshwater before the freshwater turns eastward upon exiting the estuary (Gan et al., 2009b). A strong SCM at about 40 m depth extends shoreward from the outer shelf to the inner shelf where the surface phytoplankton blooms of the bulge occur. The SCM shoals to about 20 m in nearshore waters as a result of upwelling. As the plume is advected eastward and seaward (Fig. 2a) by the upwelling current, the surface bloom in the plume extends to far field. Unlike in section A, the SCM in section B disappears shoreward from the offshore edge of the surface plume. This is shown in both the observed and the simulated fields. Section C is located at the southwestern corner of the Taiwan Shoals. The bloom in the water column shoreside of the Shoals is cut-off from the SCM seaside of the Shoals and there is virtually no SCM formation over the shelf on the shoreside due to strong mixing (Gan et al., 2009a). The source of the nearshore bloom in section C is the upwelled deep water along the section B where the head of a widened shelf exists as shown by Gan et al. (2009a, 2010).

Fig. 3b summarizes the spatial variation of the depth and intensity of the SCM at depths greater than 40 m over the entire shelf of the NSCS. Generally, the depth of the SCM decreases shoreward while its intensity weakens. Relatively shallow (<40 m) and weak SCM (<1.5 μg L^{-1}) are found in the waters shoreward of the 50 m isobath, where the strong coastal upwelling and high concentration of Chl a of the river plume are located. Offshore of the 50 m isobath, the depth of the SCM remains around 40 m, and its intensity is about 2 μg L^{-1}. A number of studies also reported similar SCM variation patterns over the continental shelf of the NSCS. Cai et al. (2002) observed a strong SCM with an average value of 3.2 ± 1.8 μg L^{-1} in the waters from 50 to 75 m during the summer of 1999; Peng et al. (2006), however, showed a relatively lower value of 0.81 ± 0.43 μg L^{-1} in the coastal zone and 1.14 ± 1.65 μg L^{-1} in shelf waters. Our results indicate that the SCM is largely affected by the highly variable physical and biological processes of the upwelling circulation and the river plume especially in nearshore waters. The field observations show that the SCM is generally formed near the halocline/thermocline where the availability of nutrient and light are favorable for an SCM. Despite its spatial variability, SCM contributes significant biological productivity in the NSCS. Our calculation shows that the primary production in the SCM is about 65% of those in the plume and upwelled waters over the domain of Fig. 3b.

To further analyze the correlation between the SCM and the vertical structure of related physical/biogeochemical parameters, vertical profiles of observed and simulated density, NO_3 and chlorophyll are plotted at two stations in the outer shelf (Sta. A3) and the inner shelf (Sta. A8) (Fig. 4), respectively. Both the observed and simulated SCMs in these two stations were formed at the top of the nutricline, suggesting that nutrient availability plays a dominant role in the formation of the SCM in this region. As an oligotrophic sea, nutrient limitation (mainly nitrogen limitation) for phytoplankton growth in the SCS has been reported (Wu et al., 2003).

4. Analysis and discussion

Besides physically raising the SCM, wind-driven upwelling also greatly enhances vertical mixing in the water column. An intense phytoplankton bloom in the plume may affect the SCM beneath it by altering the intensity of PAR. In this section, the formation and maintenance mechanisms of the SCM, under the influence of upwelling shelf circulation and the associated river plume in the NSCS, are investigated by using both field measurements and a set of modeling sensitivity experiments.
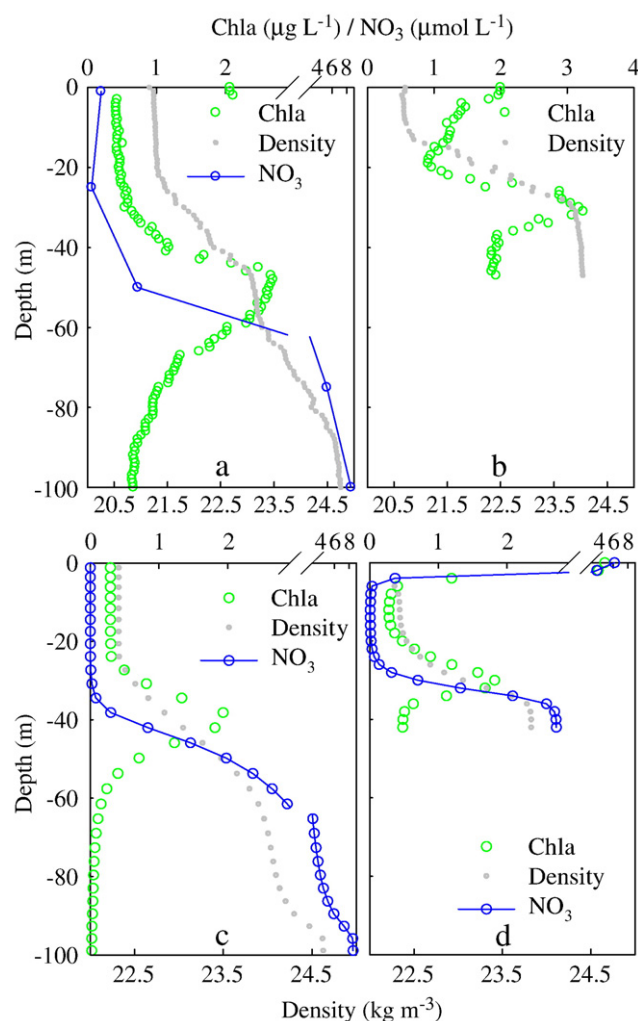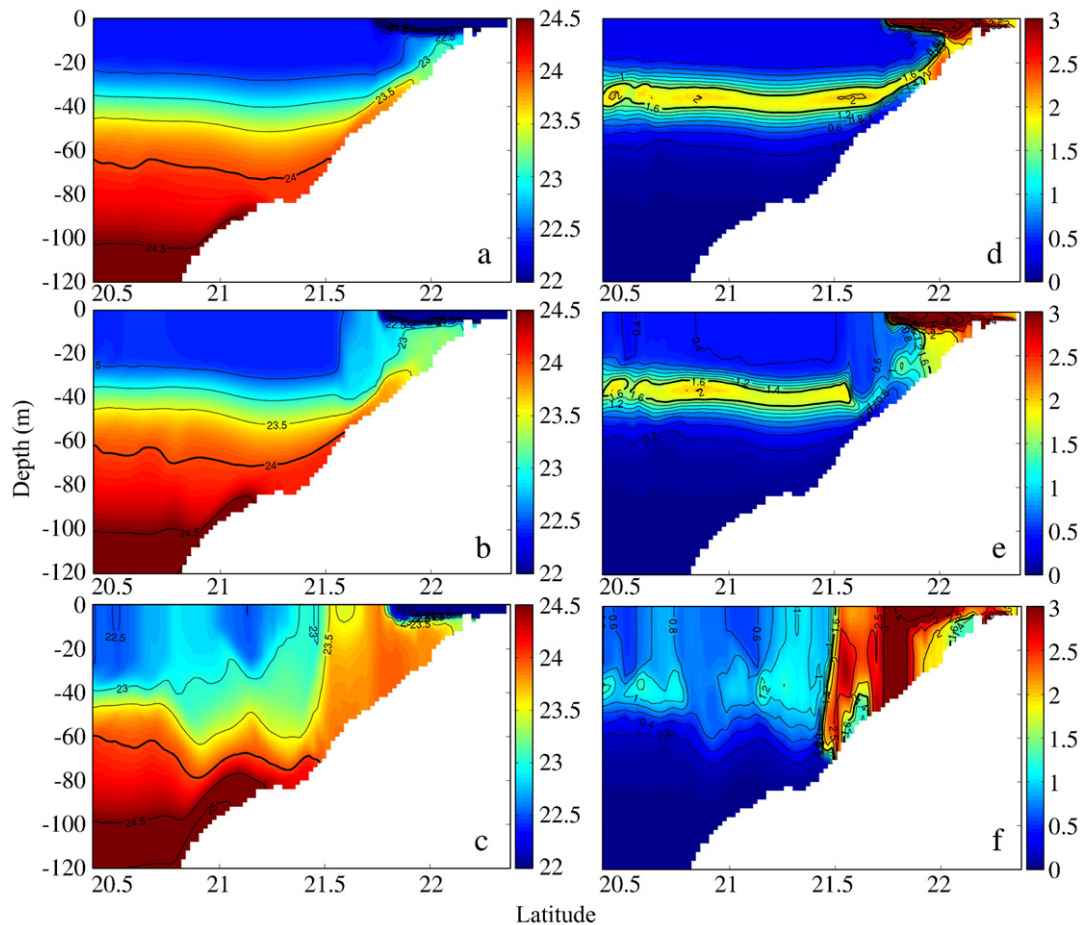

Fig. 4. The upper panel shows the observed (Jul. 20–21 2004) density and Chl a profiles at (a) offshore A3 and (b) nearshore A8 stations along section A. The lower panel shows the corresponding simulated results at the same stations.

Fig. 5. Density (kg m^{-3}) (left panel) and chlorophyll (μg L^{-1}) (right panel) distributions in section A forcing with wind stresses of (a, d) 0.025 Pa, (b, e) 0.05 Pa, and (c, f) 0.1 Pa, respectively.

4.1. Response to the upwelling favorable wind

A stable and stratified water column is favorable for the formation and maintenance of the SCM, because the high concentration of chlorophyll in the SCM layer will be less likely diluted by the relatively low-chlorophyll ambient waters. During upwelling in the NSCS, turbulent kinetic energy imparted by wind stress will weaken the stability and stratification of the upper water column. To assess the impact of wind stress on the formation and maintenance of the SCM, a set of sensitivity experiments with wind stresses of 0.025 Pa, 0.05 Pa, and 0.1 Pa were conducted. The response of all the physical/biogeochemical parameters share similar patterns in cross-sections A, B, and C. Thus, the cross-section distributions of density and chlorophyll in section A is selected to illustrate the effect of wind stress. Fig. 5 shows that the vertical distribution of density and chlorophyll are significantly modulated by the magnitude of the wind stress. At the inner shelf, significant strengthening of coastal upwelling and vertical mixing occur as the magnitude of upwelling favorable wind increases (Fig. 5a–c). But the water column on the outer shelf remains relatively stable as the pycnocline remains nearly unchanged. An obvious phenomenon of the chlorophyll distribution is that the intensity of the SCM weakens with increasing wind stress, both in the outer and inner shelves. In the case with the wind stress of 0.025 Pa, the maximum value of chlorophyll in the SCM layer was around 2 μg L^{-1}, but it dropped to about 1–1.5 μg L^{-1} with a wind stress of 0.1 Pa. The nearshore SCM is also interrupted by the stronger coastal upwelling under stronger wind stress (Fig. 5e). Nevertheless, the location of the SCM remains at the same depth over the outer shelf for all the three cases, and the SCM disappears over the

inner shelf when the water column becomes unstable under wind stresses of 0.05 Pa and 0.1 Pa (Fig. 5e, f).

Fig. 6 shows the effect of wind stress on the SCM by showing the changes of the water column's stability. The intensifying vertical mixing with strengthening wind stress is clearly shown by the thickening mixed layer and by increasing/decreasing water density above/below pycnocline. The intensity of turbulent mixing, as shown by values of vertical kinematic viscosity (Fig. 6f), enhances and deepens accordingly. The bottom of mixed layer is typically located at the depth where turbulent mixing is decreasing from its peak intensity. The intensity of the SCM displays a negative correlation with the magnitude of the wind stress. The correlation coefficient is −0.978 when the intensity of the SCM is represented by the averaged Chl a within the 30–50 m layer. However, the depth of the SCM under different wind stress remains nearly unchanged, similar to the depth of the nutricline (Fig. 6c). At the same time, chlorophyll above the SCM layer (upper 20 m) increases as the magnitude of wind stress increases. The average Chl a in the upper 80 m of all the 3 cases is kept at a constant value of 0.6 ± 0.005 μg L^{-1} in the waters. The phytoplankton biomass is apparently increasing with the strengthening of wind stress, with average values of about 0.32, 0.33, and 0.38 in the upper 80 m for the three cases, respectively (Fig. 6d). The nutrients pumped to the upper layer were quickly assimilated by phytoplankton which explains the near depletion of NO$_3$ in the upper layer. The relatively constant vertically-averaged chlorophyll concentration is due to the variable chlorophyll to phytoplankton biomass ratio (Fig. 6e), in which the chlorophyll increase in the upper layer is offset by the chlorophyll decrease in the SCM layer.
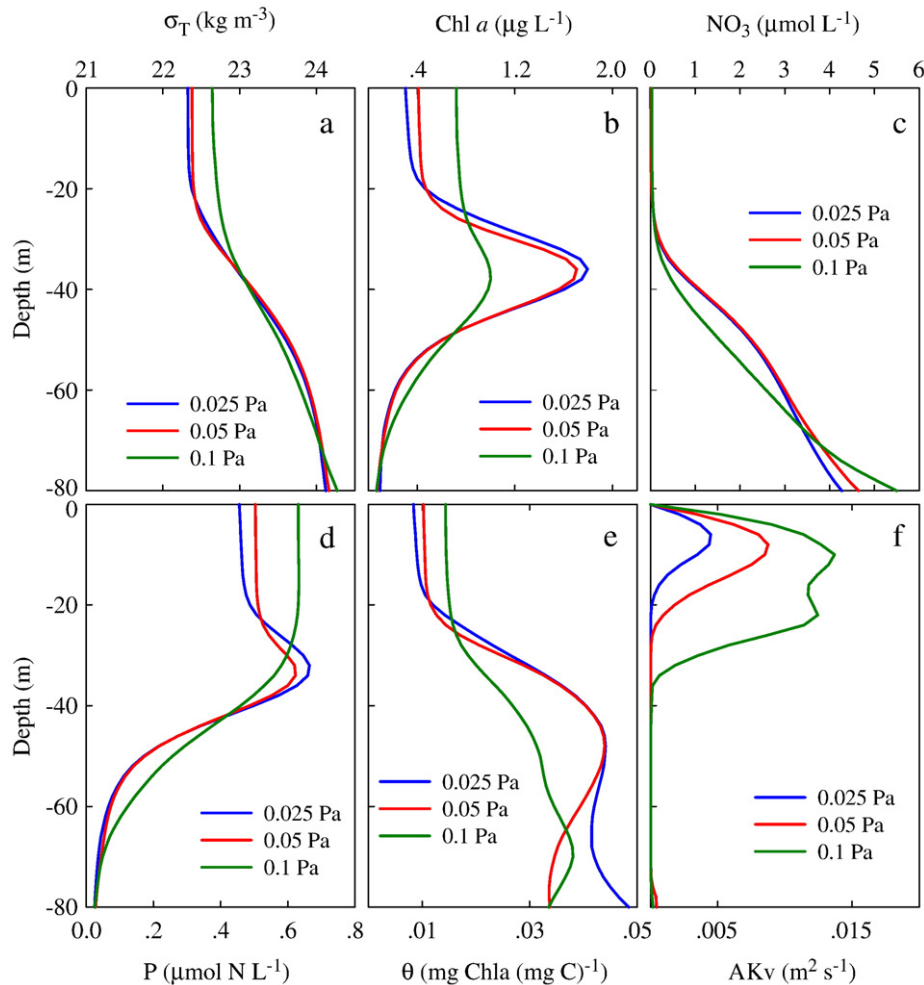
Fig. 6. Profiles of horizontally averaged (a) density (σ_T), (b) chlorophyll, (c) NO_3, (d) phytoplankton, (e) chlorophyll to phytoplankton ratio (θ), and (f) vertical kinematic viscosity (AKv) along section A forced with different wind stresses.

The sensitivity experiments demonstrate that the wind stress is an important controlling factor for the formation and maintenance of the SCM over the shelf. Wind stress modulates the nutrient transport through coastal upwelling and wind-induced mixing. The fact that the depth of the SCM remains unchanged during variable wind forcing suggests that the wind brings more nutrients and chlorophyll to the upper layer while the nutricline remains relatively stable. This is true even though the vertical mixing in the upper water column is stronger under higher wind stress. Varela et al. (1992) also found that the distribution of chlorophyll in the water column above the SCM tended to be more homogeneous while the location of the SCM remained vertically unchanged because of increasing eddy diffusion in the layer above the thermocline.

4.2. Response to the river plume and incident PAR

The weakening or disappearance of the SCM beneath the river plume is another significant feature in the NSCS. This is shown in Fig. 3a by the observed and simulated chlorophyll in section B. Observations at two single stations show the contrasting features of the SCM in response to the presence and absence of the river plume (Fig. 7). Without the influence of the plume in the surface layer at station A4, a significant SCM exists at nearly 80 m depth (Fig. 7a, b) while there is no evidence of formation of an SCM at station B3 when the plume exists (Fig. 7c, d). Although the NO_3 concentration at both stations is qualitatively and

quantitatively similar, the PAR exhibits a faster decreasing rate with depth at station B3 than at station A4 (Fig. 7a, c).

The control of PAR on the SCM is governed by equations A_7, A_8, A_{10}, and A_{11} in Appendix A. The equations show the relationship among phytoplankton growth rate, PAR, nutrient, and chlorophyll concentration. In the model, the incident PAR is vertically attenuated with depth-dependent chlorophyll concentration as described by equation A_{11}. Thus, concentration of chlorophyll is crucial to determine the attenuation of PAR with depth if k_{water} and k_{chla} are kept constant. Numerical simulations reproduced the observed features well (Fig. 8). When the river plume is absent, about 30% of surface incident PAR remains at 30 m and a strong SCM is generated at the same depth. In contrast, only ~5% of the surface incident value is left at 30 m depth and only a weak signal of the SCM can be found (Fig. 8a, c) in the subsurface layer when the river plume exists. There are no obvious changes in vertical structures of salinity, temperature, and NO_3 below the river plume in the two cases.

Generally, before photo-inhibition occurs, phytoplankton growth is positively correlated with PAR under similar nutrient conditions. The ratio of chlorophyll to phytoplankton biomass is negatively correlated with PAR and positively correlated with nutrient concentration in the water column (Fennel and Boss, 2003). To further examine the chlorophyll vertical distribution and the response of the SCM to PAR, sensitivity experiments with surface short wave radiations of 150 W m^{-2}, 200 W m^{-2}, and 300 W m^{-2} were
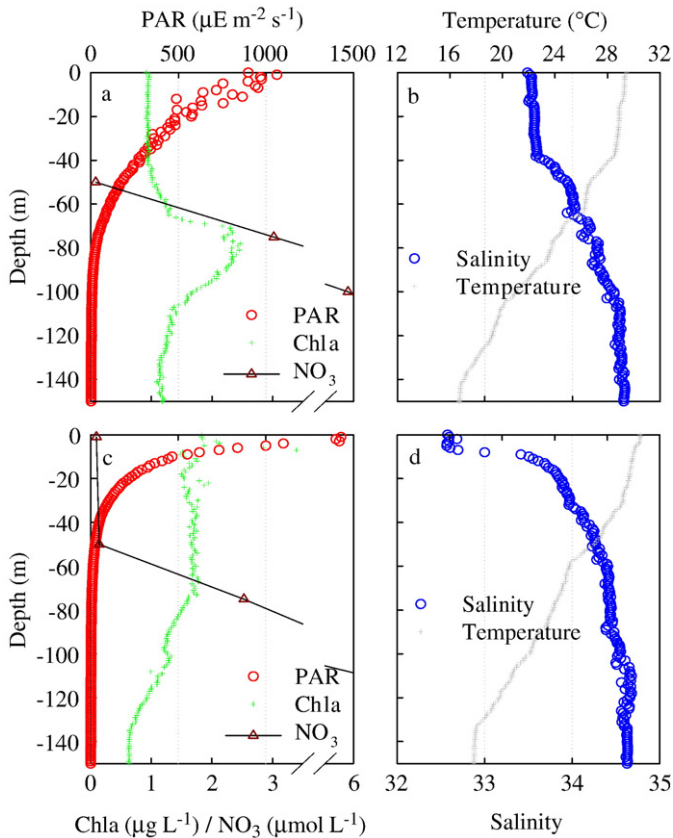
Fig. 7. Vertical profiles of (a) PAR, chlorophyll and NO$_3$, (b) salinity and temperature without river plume at station A4 obtained in July 2000; (c) and (d) are the corresponding profiles with river plume at station B3 obtained in July 2004.

phytoplankton biomass, will reach a relatively constant value under different incident PAR (Fig. 10c). Because the chlorophyll to phytoplankton ratio depends on PAR and NO$_3$, a lower chlorophyll to phytoplankton ratio occur under a higher PAR and a lower NO$_3$ concentration (Fig. 10d). Thus, the chlorophyll concentration decreases with increasing PAR in the surface layer (Fig. 10b). Generally, the concentration of NO$_3$ in the upper mixed layer (0.02–0.03 μmol L^{-1}) is about one order of magnitude lower than the half-saturation for phytoplankton uptake. Along with the increasing PAR, the SCM must then move downward until there are sufficient nutrients to sustain the growth of phytoplankton. These results indicate that the variation of the incident radiation changes the availability of PAR in the water column, and leads to the interactive response in chlorophyll concentration, nutricline and the location of the SCM.

4.3. Time-dependent variation

The interactive processes of the SCM evolution governed by the physical forcing of upwelling circulation and river plume and by the biological forcing of light, nutrient and grazing pressure in a coastal station at water depth of 30 m in section B are shown by the time series in Fig. 11.

After a short time (2–3 days) increase to consume the nutrient in the surface layer, the surface Chl a is persistently decrease before river plume arrives due to no enough nutrient supply (Fig. 11a, b). The PAR in the SCM layer, however, exhibits an inverse variation according to equation A$_{11}$. Under this favorable environment, phytoplankton
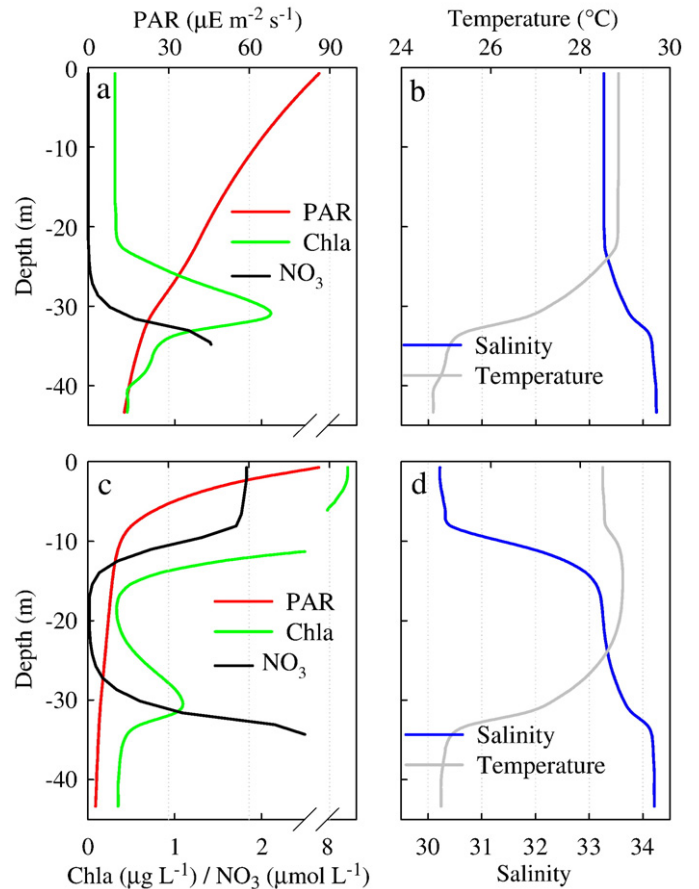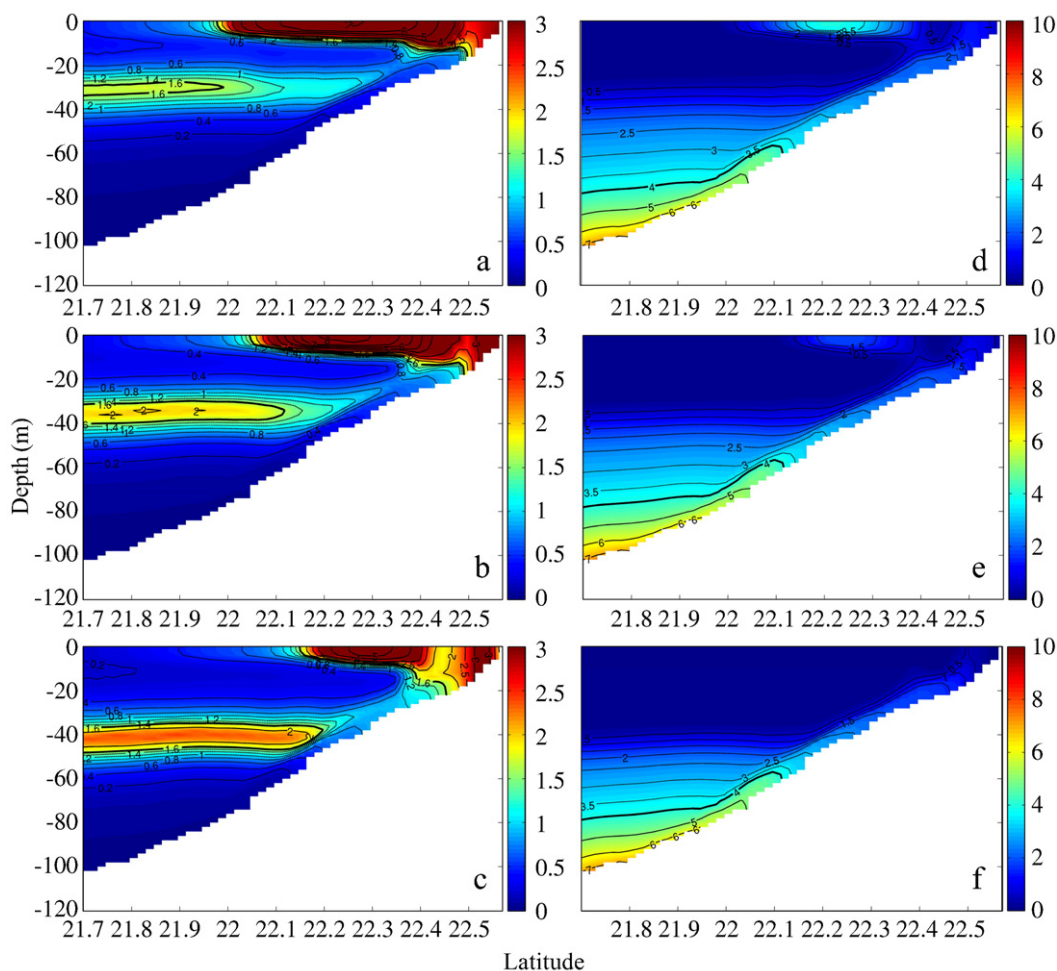
conducted. The results are illustrated by the chlorophyll and NO$_3$ vertical profiles in section B (Fig. 9). The variability in the vertical profiles of NO$_3$, chlorophyll, phytoplankton, and the ratio of chlorophyll to phytoplankton biomass, under different incident PAR at a single station in section B is also displayed in Fig. 10.

There are substantial increases of the SCM when stronger incident PAR is applied. The SCM also deepens when incident PAR increases (Fig. 9). The results suggest that both the intensity and the location of the SCM is the result of a balance between upward nutrient flux and downward light attenuation. When there are not enough nutrients but enough PAR, the growth of phytoplankton is limited by nutrients. With increasing PAR, the SCM deepens to acquire sufficient nutrients to support a higher phytoplankton biomass and growth rate.

Extracted from a single station along section B, Fig. 10 shows that increasing incident PAR deepens both the nutricline and the location of the SCM. At the same time, the chlorophyll and NO$_3$ concentration in the upper mixed layer is lower under higher incident PAR. The phytoplankton biomass under different incident PAR follows similar vertical distributions with the SCM except in the upper layer. With the same physical forcing in these sensitivity experiments, the vertical transport of NO$_3$ from the deep layer to the mixed layer is identical for each case. But, providing the nutrient concentration remains unchanged, the growth rate of phytoplankton is higher with stronger PAR according to the growth rate and its dependent photosynthesis–light relationship as shown in equations A$_7$ and A$_{10}$, respectively. Therefore, if the phytoplankton biomass is invariant, the nutrients are likely to be consumed faster under stronger PAR. When the NO$_3$ replenishment from vertical diffusion and remineralization is balanced with the depletion (mainly due to phytoplankton uptake and sinking), the phytoplankton growth rate and, consequently, the

Fig. 8. Simulated vertical profiles of (a) PAR, chlorophyll and NO$_3$, (b) salinity and temperature for the case without river discharge at a station (115.24°E, 22.25°N) in section B; (c) and (d) are the corresponding profiles for the case with river discharge.

Fig. 9. Chlorophyll (µg L^{-1}) distributions in section B with short wave radiation of (a) 150 W m^{-2}, (b) 200 W m^{-2} and (c) 300 W m^{-2}, respectively; (d), (e) and (f) are the corresponding NO$_3$ (µmol L^{-1}) distributions.

(indicated by Chl a) and zooplankton in the SCM layer keep growing while NO$_3$ is consumed (Fig. 11c, d). In general, during the first 12 days of biological adjustment from the initial fields, low biological activities occur in the oligotrophic surface layer, while the intensity of SCM gradually increases to ~2 µg L^{-1} from ~1 µg L^{-1}.

Shortly after the plume reaches the station on day 12 driven by upwelling circulation, PAR in the SCM layer decreases sharply when surface Chl a quickly increases. The intensity of SCM weakens thereafter to its original value of ~1 µg L^{-1}. Accordingly, the concentration of NO$_3$ rises due to the decreasing biological uptake (Fig. 11a, c). After day 20, the evolution reaches a dynamic equilibrium among the biological variables in the river plume (Fig. 11a) and the intensity of PAR and SCM become less fluctuated (Fig. 11c). When there is no river plume, surface Chl a, NO$_3$, and zooplankton are always low and there is no intense variation of the SCM. The biological variables maintain a dynamic equilibrium between phytoplankton growth and zooplankton grazing after reaching a relatively stable level on day 20 (Fig. 11d).

The evolutions clearly show that the biological processes which form, regulate, and maintain the SCM in the shelf waters are controlled by the upwelling circulation and plume. It also suggests that the SCM may play important role in the biological variability in the NSCS. The drastically different responses of the SCM and the associated biological variables between the cases with and without plume illustrate the variability of SCM induced by the coupled physical–biological forcing.

5. Summary and conclusion

By using both field measurements and a three dimensional coupled physical–biological model, we examined the variability of the SCM under the controls of a river plume and coastal upwelling over the continental shelf of the NSCS during summer monsoon season. Driven by idealized but representative forcing for the summer upwelling conditions, the model qualitatively well reproduces the observed characteristics of the SCMs; and this process-oriented modeling study is able to identify the key characteristics and processes of the SCM in the NSCS.

The SCMs, which has biomass comparable to those contributed by upwelled and plume waters, were found at the top of the nutricline due to the crucial control of nutrient availability to the SCM formation. Consequently, the depth and intensity of SCM are spatially variable, primarily determined by the physical and biological controls of the variable upwelling and river plume. We identified the shoaling and weakening of the SCM in the upwelling zone in nearshore waters, and the weakening or disappearance of the SCM beneath the plume waters.

The intensity of the SCM tends to be diminished due to dilution by stronger upwelling and vertical mixing under stronger wind stress, while the depth of the SCM has little variation as a result of stable nutricline except in the nearshore waters where strong upward current occurs. On the other hand, the water column integrated phytoplankton biomass tends to be higher under stronger wind stress as more nutrients
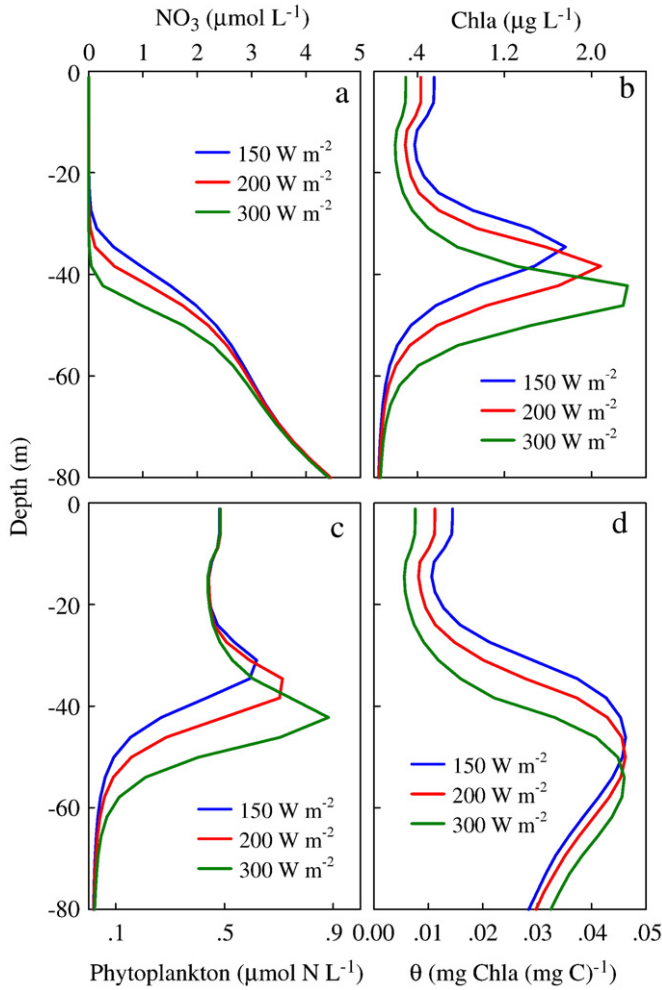
Fig. 10. Vertical profiles of (a) NO$_3$, (b) chlorophyll, (c) phytoplankton, and (d) ratio of chlorophyll to phytoplankton biomass in section B at 21.8°N under different incident PAR.

are pumped upwards by the stronger vertical mixing, while the vertically-averaged chlorophyll concentration remains relatively constant due to lower chlorophyll to phytoplankton ratio. Thus, both physically controlled dilution and biologically forced chlorophyll to phytoplankton ratio regulate the variation of SCM.

The intensity of the SCM is positively correlated with PAR. The plume water with a high concentration of chlorophyll quickly attenuates PAR in the surface layer and greatly weakens the SCM. With stronger incident PAR, the SCM deepens in order to obtain sufficient nutrients to sustain the higher growth rate of phytoplankton. At the same time, chlorophyll concentration in the upper mixed layer lessens caused by the lower chlorophyll to phytoplankton ratio under higher PAR and by the lower nutrient concentration due to stronger nutrient consumption with a higher phytoplankton growth rate. The interactive processes among the upward NO$_3$ flux and downward PAR attenuation regulate the distribution of the vertical chlorophyll profiles.

The variable SCM in the NSCS is controlled by the coupled physical–biological processes that involve upwelling circulation, river plume and associated biological balances among PAR, nutrient and planktons.

Acknowledgements

Appendix A

The time-dependent changes of biological variables in the model are governed by the following equations:

$$\frac{\partial [N]}{\partial t} = -\mu_{max} * f(I) * \frac{[N]}{k_N + [N]} * \frac{1}{1 + [A]/k_A} * [P] + n * [A] \tag{A1}$$

$$\frac{\partial [A]}{\partial t} = -\mu_{max} * f(I) * \frac{[A]}{k_A + [A]} * [P] - n * [A] + l_{BM} * [Z] \\ + l_E * \frac{[P]^2}{k_P + [P]^2} * AE_N * [Z] + r_{SD} * [SD] + r_{LD} * [LD] \tag{A2}$$

$$\frac{\partial [P]}{\partial t} = \mu * [P] - m_P * [P] - \tau * ([SD] + [P]) * [P] \\ - g_{max} * \frac{[P]^2}{k_P + [P]^2} * [Z] - w_P \frac{\partial [P]}{\partial z} \tag{A3}$$

$$\frac{\partial [Z]}{\partial t} = g_{max} * \frac{[P]^2}{k_P + [P]^2} * AE_N * [Z] - l_{BM} * [Z] \\ - l_E * \frac{[P]^2}{k_P + [P]^2} * AE_N * [Z] - m_Z * [Z]^2 \tag{A4}$$

$$\frac{\partial [SD]}{\partial t} = g_{max} * \frac{[P]^2}{k_P + [P]^2} * (1 - AE_N 1 - AE_N) * [Z] + m_Z * [Z]^2 \\ + m_P * [P] - \tau * ([SD] + [P]) * [SD] - r_{SD} * [SD] - w_{SD} \frac{\partial [SD]}{\partial z} \tag{A5}$$

$$\frac{\partial [LD]}{\partial t} = \tau * ([SD] + [P])^2 - r_{LD} * [LD] - w_{LD} * \frac{\partial [LD]}{\partial z} \tag{A6}$$

Where μ denotes the growth rate of phytoplankton and is defined as:

$$\mu = \mu_{max} * f(I) * \left(\frac{[N]}{k_N + [N]} * \frac{1}{1 + [A]/k_A} + \frac{[A]}{k_A + [A]} \right) \tag{A7}$$

$$\mu_{max}(T) = \mu_0 \cdot 1.066^T \tag{A8}$$

Where μ_{max} is the maximum growth rate of phytoplankton, N is nitrate, K_N is half-saturation for phytoplankton NO$_3$ uptake, A is ammonium, K_A is half-saturation for phytoplankton NH$_4$ uptake, T is temperature. μ_0, the phytoplankton growth rate is 0.59.

n is the nitrification (NH$_4^+$ + 2O$_2$ → NO$_3^-$ + 2H$^+$ + 2H$_2$O) rate that is regulated by light (Olson, 1981) and governed by the equation:

$$n = n_{max} * \left(1 - \max \left[0, \frac{I - I_0}{k_I + I - I_0} \right] \right) \tag{A9}$$

In which n_{max} is the maximum nitrification rate, I_0 is the radiation threshold for nitrification inhibition, and k_I is the half-saturation radiation for nitrification inhibition.
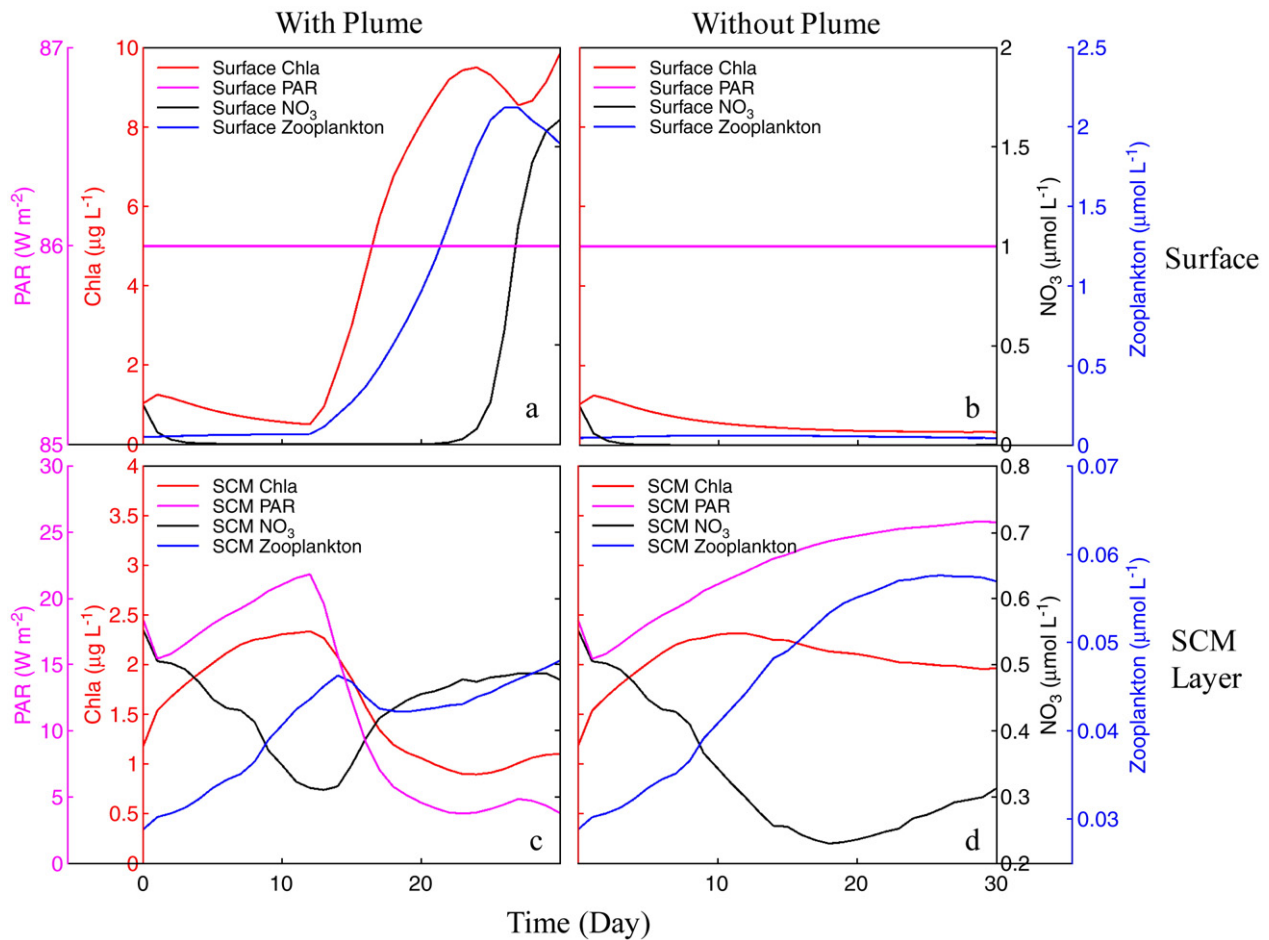
Fig. 11. Time-series evolution of Chl *a*, PAR, NO₃, and zooplankton (a, b) in the surface layer and (c, d) in the SCM layer at the same station of Fig. 8. The left and right panels are for the cases with and without river discharge, respectively.

The function $f(I)$ represents the photosynthesis–light (P–I) relationship:

$$f(I) = \frac{\alpha I}{\sqrt{\mu_{max}^2 + \alpha^2 I^2}} \tag{A10}$$

$$I = I(z) = I_0 * par * \exp \left\{ -z * \left(K_{water} + K_{chla} * \int_z^0 Ch(\varsigma) d\varsigma \right) \right\} \tag{A11}$$

where I is the same as *PAR*, I_0 is the incoming light just below the sea surface, α is the initial slope of the *P–I* curve, *par* is the fraction of light that is available for photosynthesis and equals 0.43, K_{water} is the light attenuation coefficient for seawater, K_{chla} is the light attenuation coefficient for chlorophyll.

A nonlinear relationship between chlorophyll and phytoplankton biomass is applied in this model to reflect the acclimation to changes in light and nutrient conditions (Fennel et al., 2006). The model equation of chlorophyll can be written as:

$$\frac{\partial [Chla]}{\partial t} = \rho_{Chla} * \mu * [Chla] - m_P * [Chla] - \tau * ([SD] + [P]) * [Chla]$$
$$- g_{max} * \frac{[P]^2}{k_P + [P]^2} * [Z] * \frac{[Chla]}{[P]} \tag{A12}$$

In which ρ_{Chla} is the fraction of phytoplankton growth that devoted to chlorophyll synthesis, which is defined as:

$$\rho_{Chla} = \frac{\theta_m * \mu * [P]}{\alpha * I * [Chla]} \tag{A13}$$

Appendix B

Biogeochemical model parameters

Description	Symbol	Value	Units
Light attenuation due to seawater	k_{water}	0.04	m^{-1}
Light attenuation by chlorophyll	k_{Chla}	0.025	$(m^2\,mg\,Chla)^{-1}$
Initial slope of the P–I curve	α	0.025	mg C $(mg\,Chla\,W\,m^{-2}\,d)^{-1}$
Maximum cellular chlorophyll : C Ratio	θ_m	0.054	mg Chla $(mg\,C)^{-1}$
Half-saturation for phytoplankton NO₃ uptake	K_N	0.5	mmol N m^{-3}
Half-saturation for phytoplankton. NH₄ uptake	K_A	0.5	mmol N m^{-3}
Phytoplankton mortality rate	m_P	0.15	d^{-1}
Zooplankton maximum grazing rate	g_{max}	0.6	d^{-1}
Zooplankton assimilation efficiency for Nitrogen	AE_N	0.75	–
Zooplankton half-saturation constant for ingestion	K_P	1	mmol N m^{-3}
Zooplankton basal metabolism	l_{BM}	0.1	d^{-1}
Zooplankton specific excretion rate	L_E	0.1	d^{-1}
Zooplankton mortality rate	m_Z	0.025	d^{-1} $(mmol\,N\,m^{-3})^{-1}$
Small detritus remineralization rate	r_{SD}	0.03	d^{-1}
Large detritus remineralization rate	r_{LD}	0.01	d^{-1}
Coagulation rate	τ	0.05	d^{-1}
Sinking velocity for small detritus	w_{SD}	0.1	$m\,d^{-1}$
Sinking velocity for large detritus	w_{LD}	1	$m\,d^{-1}$
Sinking velocity for Phytoplankton	w_P	0.1	$m\,d^{-1}$
Maximum nitrification rate	n_{max}	0.05	d^{-1}
Threshold PAR for nitrification inhibition	I_0	0.0095	W m^{-2}
Half-saturation PAR for nitrification inhibition	k_I	0.036	W m^{-2}

References

Anderson, G.C., 1969. Subsurface chlorophyll maximum in the Northeast Pacific Ocean. Limnology and Oceanography. 14 (3), 386–391.

Bienfang, P.K., 1980. Phytoplankton sinking rates in oligotrophic waters off Hawaii, USA. Marine Biology 61, 69–77.

Cai, W.J., Dai, M.H., Wang, Y.C., Zhai, W.D., Huang, T., Chen, S.T., Zhang, F., Chen, Z.Z., Wang, Z.H., 2004. The biogeochemistry of inorganic carbon and nutrients in the Pearl River estuary and the adjacent Northern South China Sea. Continental Shelf Research 24 (12), 1301–1319.

Cai, Y., Ning, X., Liu, C., 2002. Distribution characteristics of size-fractionated chlorophyll a and productivity of phytoplankton in the Northern South China Sea and Beibu Gulf during August 1999. Studia Marina Sinica 44, 11–21 in Chinese.

Chen, D., Horrigan, S.G., Wang, D.P., 1988. The late summer vertical nutrient mixing in Long-Island-Sound. Journal of Marine Research 46 (4), 753–770.

Cullen, J.J., 1982. The deep chlorophyll maximum—comparing vertical profiles of chlorophyll-a. Canadian Journal of Fisheries and Aquatic Sciences 39 (5), 791–803.

Estrada, M., 1985. Deep phytoplankton and chlorophyll maxima in the Western Mediterranean. In: Moraitou-Apostolopoulou, M., Kiortsis, V. (Eds.), Mediterranean Marine Ecosystems. Plenum Press, New York, pp. 247–277.

Fasham, M.J.R., Ducklow, H.W., McKelvie, S.M., 1990. A nitrogen-based model of plankton dynamics in the oceanic mixed layer. Journal of Marine Research 48, 591–639.

Fennel, K., Boss, E., 2003. Subsurface maxima of phytoplankton and chlorophyll: steady-state solutions from a simple model. Limnology and Oceanography 48 (4), 1521–1534.

Fennel, K., Wilkin, J., Levin, J., Moisan, J., O'Reilly, J., Haidvogel, D., 2006. Nitrogen cycling in the Middle Atlantic Bight: results from a three-dimensional model and implications for the North Atlantic nitrogen budget. Global Biogeochemical Cycles 20 (3), GB3007. doi:10.1029/2005GB002456.

Flos, J., Tintore, J., 1990. Summer frontal contribution to the fertilization of oceanic waters off the northeast coast of Spain. Oceanologica Acta 13 (1), 21–30.

Furuya, K., 1990. Subsurface chlorophyll maximum in the Tropical and Subtropical Western Pacific-Ocean - vertical profiles of phytoplankton biomass and its relationship with chlorophyll-a and particulate organic-carbon. Marine Biology 107 (3), 529–539.

Gan, J.P., Cheung, A., Guo, X.G., Li, L., 2009a. Intensified upwelling over a widened shelf in the northeastern South China Sea. Journal of Geophysical Research-Oceans 114. doi:10.1029/2007jc004660.

Gan, J.P., Li, L., Wang, D.X., Guo, X.G., 2009b. Interaction of a river plume with coastal upwelling in the northeastern South China Sea. Continental Shelf Research 29 (4), 728–740. doi:10.1016/j.csr.2008.12.002.

Gan, J.P., Lu, Z.M., Dai, M.H., Cheung, A., Harrison, P., Liu, H.B., 2010. Biological response to an intensified upwelling over a widened shelf and a river plume in the northeastern South China Sea: a modeling study. Journal of Geophysical Research. doi:10.1029/2009jc005569.

Haidvogel, D.B., Arango, H., Budgell, W.P., Cornuelle, B.D., Curchitser, E., Di Lorenzo, E., Fennel, K., Geyer, W.R., Hermann, A.J., Lanerolle, L., Levin, J., McWilliams, J.C., Miller, A.J., Moore, A.M., Powell, T.M., Shchepetkin, A.F., Sherwood, C.R., Signell, R.P., Warner, J.C., Wilkin, J., 2008. Ocean forecasting in terrain-following coordinates: formulation and skill assessment of the Regional Ocean Modeling System. Journal of Computational Physics 227 (7), 3595–3624.

Holloway, G., Denman, K., 1989. Influence of internal waves on primary production. Journal of Plankton Research 11 (2), 409–413.

Huisman, J., Thi, N.N.P., Karl, D.M., Sommeijer, B., 2006. Reduced mixing generates oscillations and chaos in the oceanic deep chlorophyll maximum. Nature 439 (7074), 322–325.

Kononen, K., Hallfors, S., Kokkonen, M., Kuosa, H., Laanemets, J., Pavelson, J., Autio, R., 1998. Development of a subsurface chlorophyll maximum at the entrance to the Gulf of Finland, Baltic Sea. Limnology and Oceanography 43 (6), 1089–1106.

Mellor, G.L., Yamada, T., 1982. Development of a turbulence closure-model for geophysical fluid problems. Reviews of Geophysics 20 (4), 851–875.

Murty, V.S.N., Gupta, G.V.M., Sarma, V.V., Rao, B.P., Jyothi, D., Shastri, P.N.M., Supraveena, Y., 2000. Effect of vertical stability and circulation on the depth of the chlorophyll maximum in the Bay of Bengal during May–June, 1996. Deep-Sea Research Part I-Oceanographic Research Papers. 47 (5), 859–873.

Ning, X., Chai, F., Xue, H., Cai, Y., Liu, C., Shi, J., 2004. Physical–biological oceanographic coupling influencing phytoplankton and primary production in the South China Sea. Journal of Geophysical Research-Oceans 109 (C10). doi:10.1029/2004JC002365.

Olson, R.J., 1981. Differential photoinhibition of marine nitrifying bacteria—a possible mechanism for the formation of the primary nitrite maximum. Journal of Marine Research 39 (2), 227–238.

Parslow, J.S., Boyd, P.W., Rintoul, S.R., Griffiths, F.B., 2001. A persistent subsurface chlorophyll maximum in the Interpolar Frontal Zone south of Australia: seasonal progression and implications for phytoplankton–light–nutrient interactions. Journal of Geophysical Research-Oceans 106 (C12), 31543–31557.

Peng, X., Ning, X., Sun, J., Le, F.F., 2006. Response of phytoplankton growth on nutrient enrichments in the northern South China Sea. Acta Ecologica Sinica 26 (12), 3959–3968 in Chinese.

Riley, G.A., Stommel, H., Bumpus, D.F., 1949. Quantitative ecology of the plankton of the western north Atlantic. Bulletin of Bingham Oceanographic Collection 12, 1–169.

Shchepetkin, A.F., McWilliams, J.C., 2005. The regional oceanic modeling system (ROMS): a split-explicit, free-surface, topography-following-coordinate oceanic model. Ocean Modelling 9 (4), 347–404.

Spitz, Y.H., Allen, J.S., Gan, J., 2005. Modeling of ecosystem processes on the Oregon shelf during the 2001 summer upwelling. Journal of Geophysical Research-Oceans 110 (C10), C10S17. doi:10.1029/2005JC002870.

Steele, J.H., 1964. A study of production in the Gulf of Mexico. Journal of Marine Research 22 (3), 211–222.

Steele, J.H., Yentsch, C.H., 1960. The vertical distribution of chlorophyll. Journal of the Marine Biological Association of the United Kingdom 39, 217–226.

Takahashi, M., Hori, T., 1984. Abundance of picophytoplankton in the subsurface chlorophyll maximum layer in subtropical and tropical waters. Marine Biology 79, 177–186.

Varela, R.A., Cruzado, A., Tintore, J., Ladona, E.G., 1992. Modeling the deep-chlorophyll maximum—a coupled physical–biological approach. Journal of Marine Research 50 (3), 441–463.

Wu, J.F., Chung, S.W., Wen, L.S., Liu, K.K., Chen, Y.L.L., Chen, H.Y., Karl, D.M., 2003. Dissolved inorganic phosphorus, dissolved iron, and Trichodesmium in the oligotrophic South China Sea. Global Biogeochemical Cycles 17, 1008. doi:10.1029/2002GB001924.